ELECTRONIC SUPPLEMENTARY INFORMATION

Bridging the thermodynamics and kinetics of temperature-induced morphology evolution in polymer/fullerene organic solar cell bulk heterojunction

Artem Levitsky[1], Sebastian Alexander Schneider[2,3], Eugen Rabkin[1], Michael F. Toney[2,4] and Gitti L. Frey[1*]

[1]*Department of Material Science and Engineering, Technion Israel Institute of Technology, Haifa 3200003, Israel*
[2]*Stanford Synchrotron Radiation Lightsource, SLAC National Accelerator Laboratory, 2575 Sand Hill Road, Menlo Park, CA 94025, USA*
[3] *Department of Chemistry, Stanford University, Stanford, California 94305-4125, United States*
[4]*Department of Chemical and Biological Engineering, University of Colorado, Boulder, CO 80309, United States*

* Corresponding Authors: gitti@technion.ac.il;

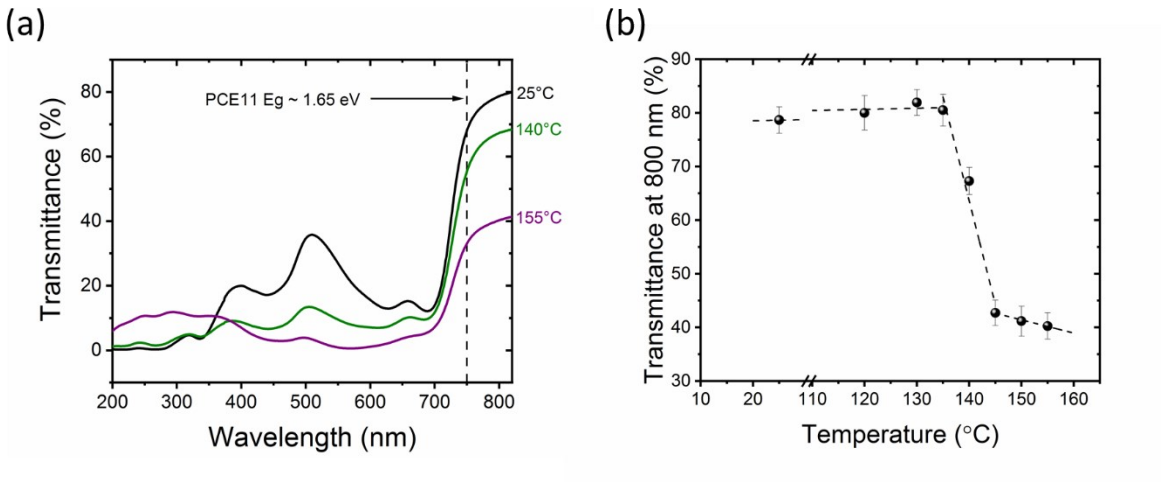

Fig. S1 (a) The transmittance spectra of 300 nm thick films of PCE11:PCBM 1:1.2 w:w spun on quartz substrates before (25°C) and after annealing for 5 min at 140°C and 155°C. The dashed line marks the band gap of the donor. Below this energy there is no donor absorption.[1] The reduction in transmittance in this range (wavelength > 750 nm), is due to scattering. (b) The transmittance at 800 nm of a PCE11:PCBM film after isothermal annealing steps, 5 min each, from 25 to 160 °C. The dashed lines represent a linear fit to the data points to indicate the transmittance signal drop when approaching the blend's Tg.

S1. Determining the glass transition temperature of the blend

Bernardo *et al.* measured Tg ~ 92 °C for the PCE11 polymer by following the change in the thermal expansion coefficient.[2] Considering the Tg variation with the Mn, provided by the Flory-Fox equation, we estimate that the Tg of the polymer used in this study is slightly higher.[3] The Tg of PCBM is reported in the literature between 110 – 140 °C.[4] Hence the Tg of the 1:1.2 blend, estimated from the Fox equation, should lie between 100 to 130 °C.[3] Ro *et al.* estimated the Tg of the 1:1.2 PCE11:Phenyl-C71-butyric acid methyl ester (PC70BM, the larger fullerene derivative with Tg ~ 163 °C) blend from differential scanning calorimetry measurements, to be in the 110 – 140 °C range,[5] in a good agreement with our estimation for PCE11:PCBM.

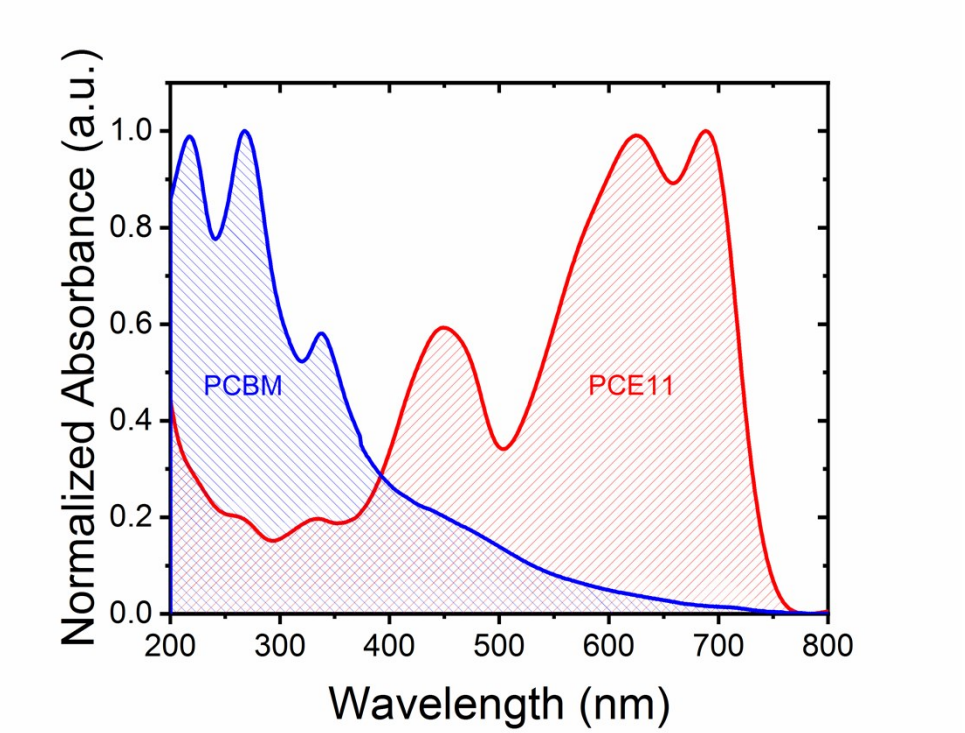

Fig. S2 Normalized absorbance spectra of a 100 nm PCBM (blue) and 300 nm PCE11 (red) films spun on quartz substrates.

S2. Deviation of NSL figure of merit

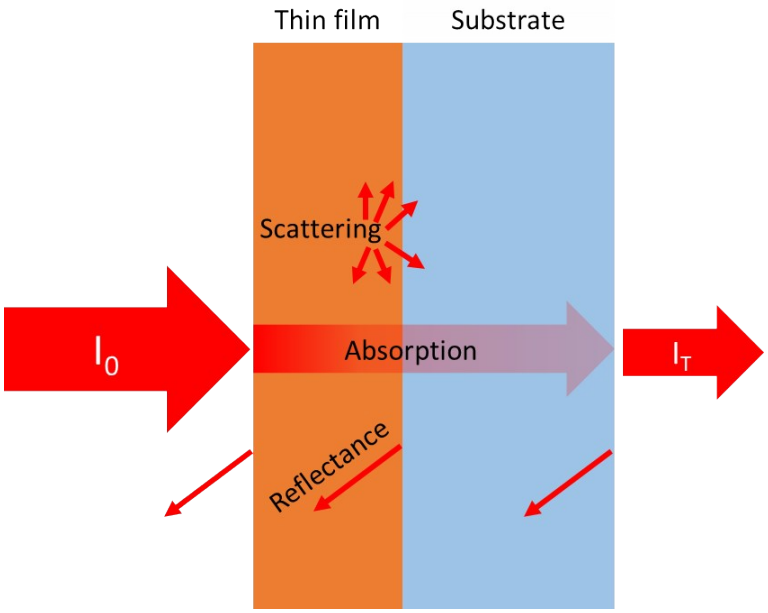

Fig. S3 Schematic representation of the optical processes that occur when light propagates through the sample.

To express the traversed light intensity (I_T), we made a few assumptions:

- The film and substrate do not absorb at 800 nm throughout the thermal annealing treatments, despite the local composition and morphology changes.
- Attenuation of light due to scattering is similar to that due to absorption in the fact that they are both expressed by exponential decay functions.[6]
- In the as-cast samples, *i.e.* t = 0 min, there are no scattering centers.

Following the above assumptions, the ratio between the transmitted light, I_T, and the incident light, I_0, is expressed by:

$$\frac{I_T}{I_0}(t) = T_1 exp(-\propto_1 L_1) exp(-N\sigma L_1) T_2 exp(-\propto_2 L_2) T_3 \qquad \text{(S1)}$$

Where I_T is transmitted light intensity, I_0 is the incident light intensity, t represent the annealing time, T_i is the coefficient of transmission by i interface, α_i is the absorption coefficient of medium i, L_i is the thickness of medium i, N is the density of scattering centers, σ is the average scattering cross-section of the scattering center. The ratio of the transmitted light and the incident light is the definition of the transmittance (not to be confused with the coefficient of transmission, T_i):

$$T(t) \equiv \frac{I_T}{I_0}(t) \tag{S2}$$

At $\lambda = 800\ nm$ the absorbance of both thin film and the quartz substrate are 0, therefore:

$$\alpha_1(800nm) = \alpha_2(800nm) = 0 \tag{S3}$$

By substituting expressions S2 and S3 into S1, the transmittance can be written as:

$$T(t) = T_1 T_2 T_3 exp(-N\sigma L_1) \tag{S4}$$

We assumed that there are no scattering centers in fresh samples, therefore we can substitute $N = 0$ for samples preceding the annealing, so expression S4 at $t = 0$ is:

$$T(t = 0) = T_1 T_2 T_3 \tag{S5}$$

Hence the product of all transmission coefficients in expression S4 can be replaced by $T(t = 0)$:

$$\frac{T(t)}{T(0)} = exp(-N\sigma L_1) \tag{S6}$$

Finally, the figure of merit NSL represent the $N\sigma L_1$:

$$NSL \equiv N\sigma L = -ln\left(\frac{T(t)}{T(0)}\right) \tag{S7}$$

And considering

$$A = -\log_{10}(T) \tag{S8}$$

Then NSL can be expressed by absorbance:

$$NSL = ln(10)(A(t) - A(0)) \approx 2.3(A(t) - A(0)) \tag{S9}$$

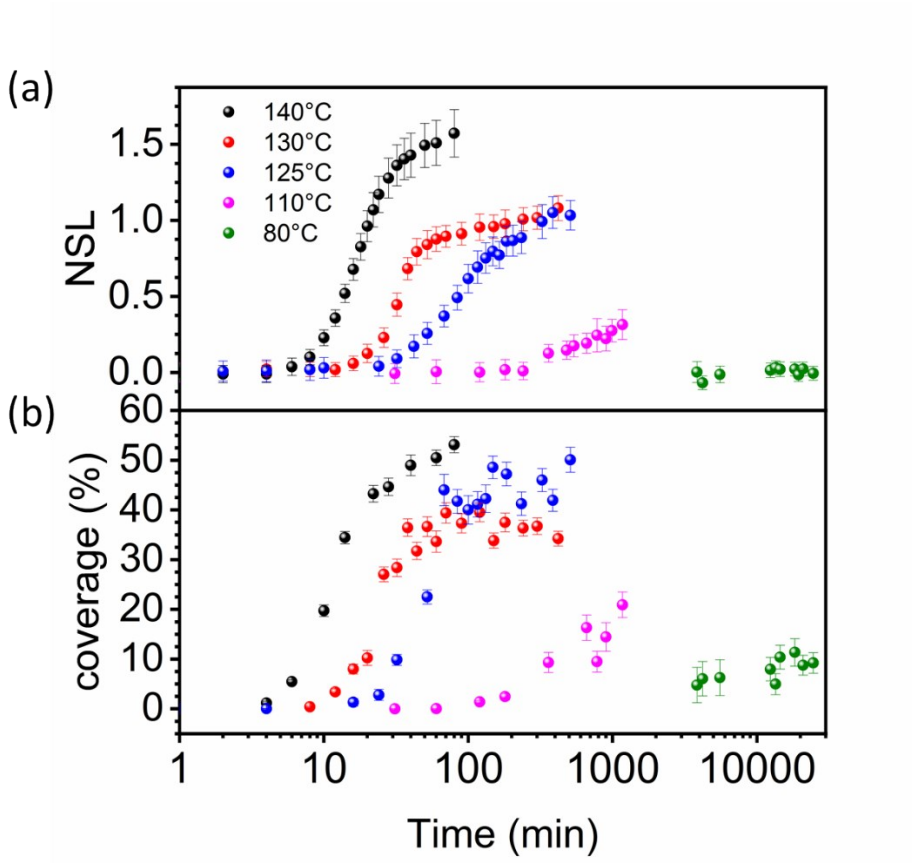

Fig. S4 Following the evolution of PCBM aggregates in 300 nm thick films of PCE11:PCBM 1:1.2 w:w during isothermal annealing by: (a) NSL, and (b) the area covered by PCBM aggregates in the optical micrographs in Fig. 1b.

S3. Sharp - Hancock plot

The Avrami equation (eqn 2) can be mathematically modified to:

$$ln\left\{-ln\left[1-\frac{NSL(t)}{NSL_{\infty}}\right]\right\}=nln(t)+nln(k) \quad \text{(S10)}$$

A plot of log[log(1⁄(1-NSL))] against log time (referred as a Sharp – Hancock plot) will give the Avrami n and k values, extracted from the slope and the intercept, respectively.[7,8] A Sharp – Hancock plot of NSL evolution during isothermal annealing at 125 °C, 130 °C and 140 °C is presented at Fig. S5. For low annealing temperatures (110 °C and 80 °C) the linear fitting is not accurate due to the low fractions of transformed PCBM. A closer look at the Sharp-Hancock plots reveals that they can be fitted with two lines, one corresponding to the initial stages of the transformation, and the second, with a smaller slope, to the later stages. The Avrami exponent values (n) and rate constants (k) were extracted from the line corresponding to the initial stages of the transformation. Generally, the change of the slope between the initial and later stages of the transformation is explained by "site saturation" – there are no sites available for nucleation and hence nucleation rate diminishes.[9] To note, we also performed similar calculations of the Avrami parameters using Sharp – Hancock plots for the area coverage of aggregates obtained from the optical micrographs in Fig. 1b (Fig. S4b).

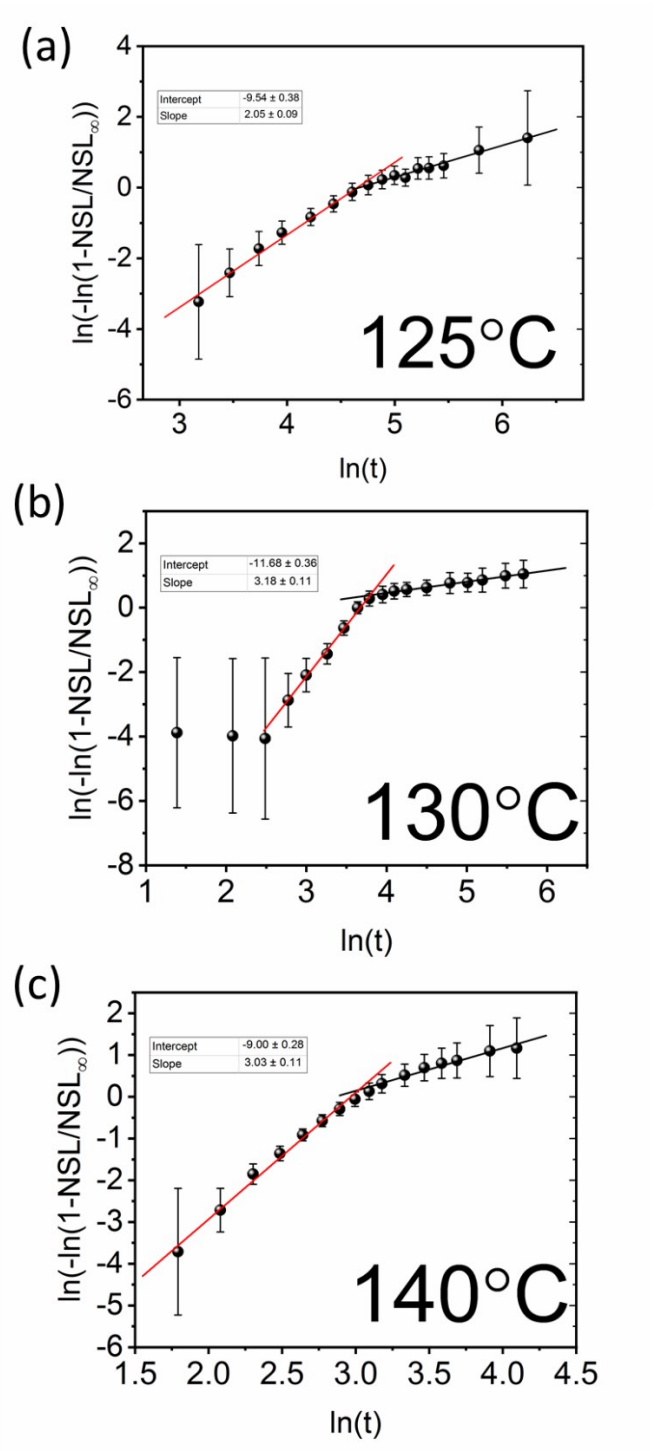

Fig. S5 Sharp – Hancock plots of NSL evolution during isothermal annealing at: (a) 125 °C, (b) 130 °C and (c) 140 °C. The Avrami parameters, i.e. Avrami exponent and rate constant, were extracted from the slope and intercept of the linear fits, respectively.

The n values related to the higher annealing temperatures (130 and 140 °C) are close to 3, while the n value extracted for the 125 °C annealing process is about 2. Assuming constant nucleation rate of crystalline PCBM clusters, their parabolic and diffusion-controlled growth in two dimensions results in JMAK exponent of n = 2. This situation corresponds to the lowest studied temperature of 125 °C, at which the kinetics of spinodal decomposition is sluggish and the thermodynamic conditions for nucleation of additional PCBM crystallites due to the change in composition (see Fig. 7) are not met. The slow kinetics can result from thermal annealing below Tg of the blend. Tg, as it was estimated previously, lie between 100 and 130 °C (see Section 1 in ESI). At higher temperatures (above the Tg) the rate of spinodal decomposition is sufficiently high, resulting in fast growth of concentration variations enabling nucleation of additional PCBM crystallites in the PCE11-lean regions. Formally, this can be described by the nucleation rate increasing with time, which in turns means that JMAK exponent is higher than 2.

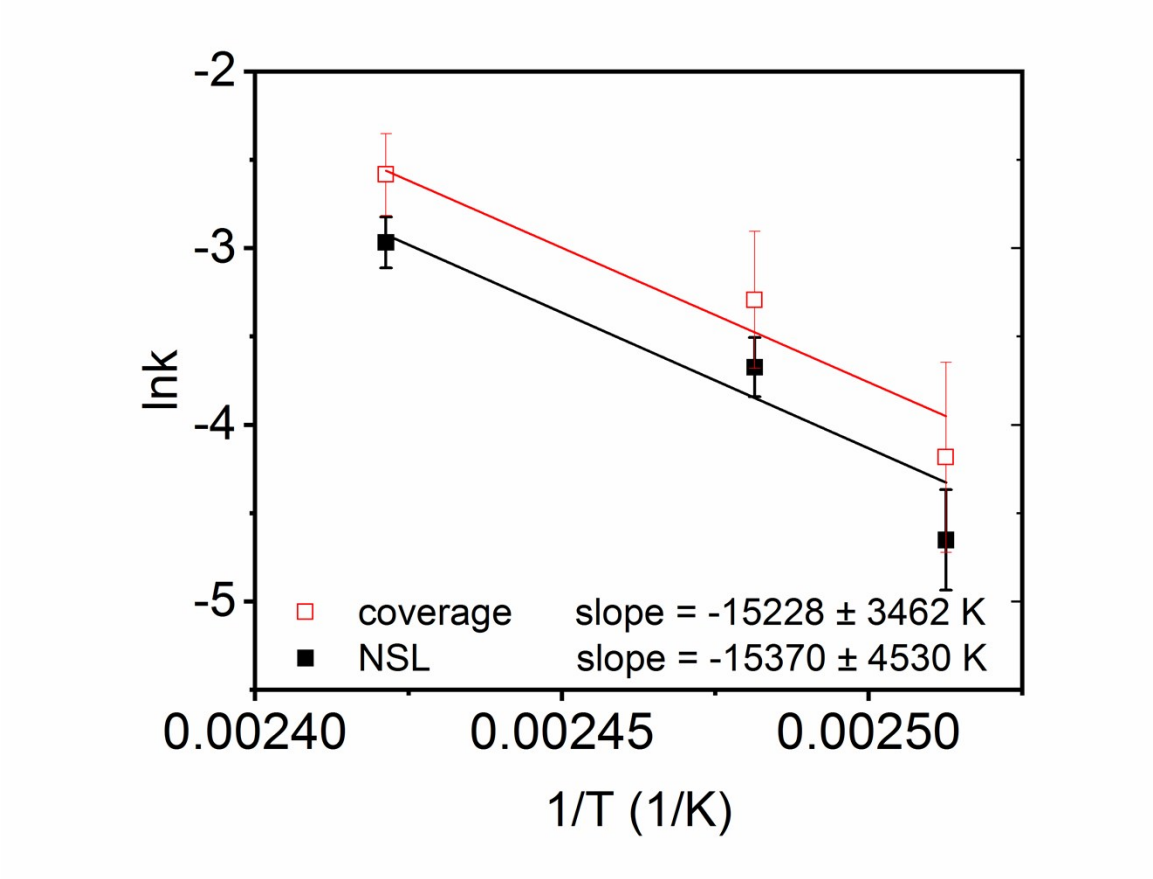

Fig. S6 Arrhenius plots of the Avrami rate constants extracted from the Sharp – Hancock plots as a function of annealing temperature. The slopes of the fitted lines are used to calculate the activation energy for PCBM aggregation (slope = $-E_a/K_B$).

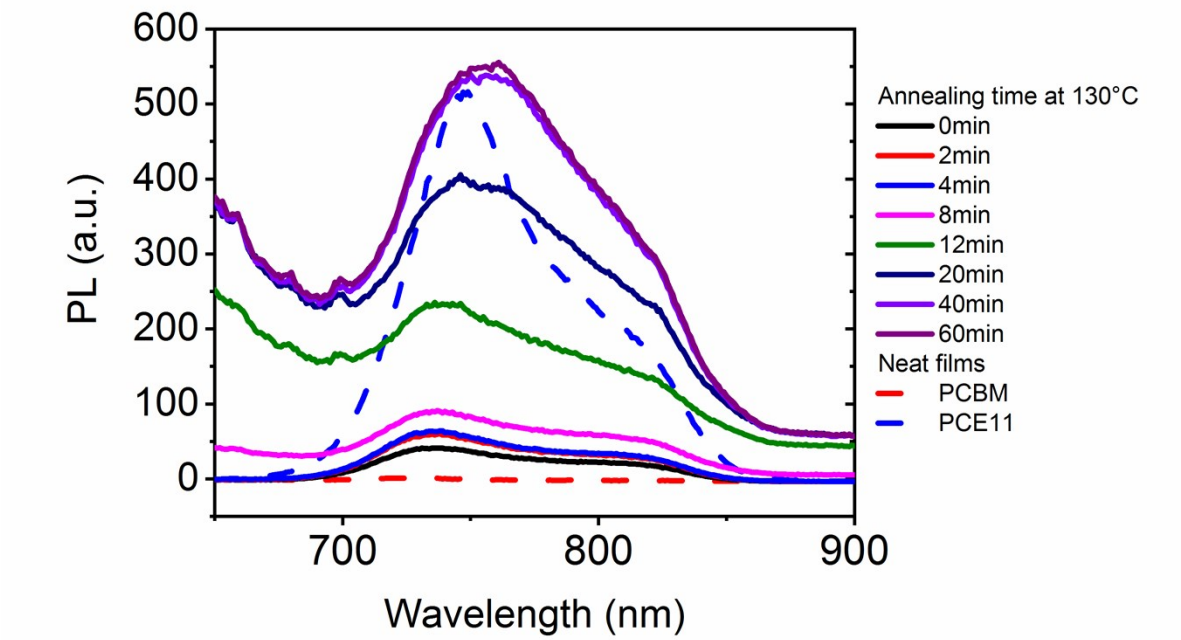

Fig. S7 Raw Photoluminescence spectra data of neat PCBM (dashed red) and PCE11 (dashed blue) films; PCE11:PCBM 1:1.2 w:w films before (0 min) and after thermal annealing at 130 °C for various times between 2 and 60 min.

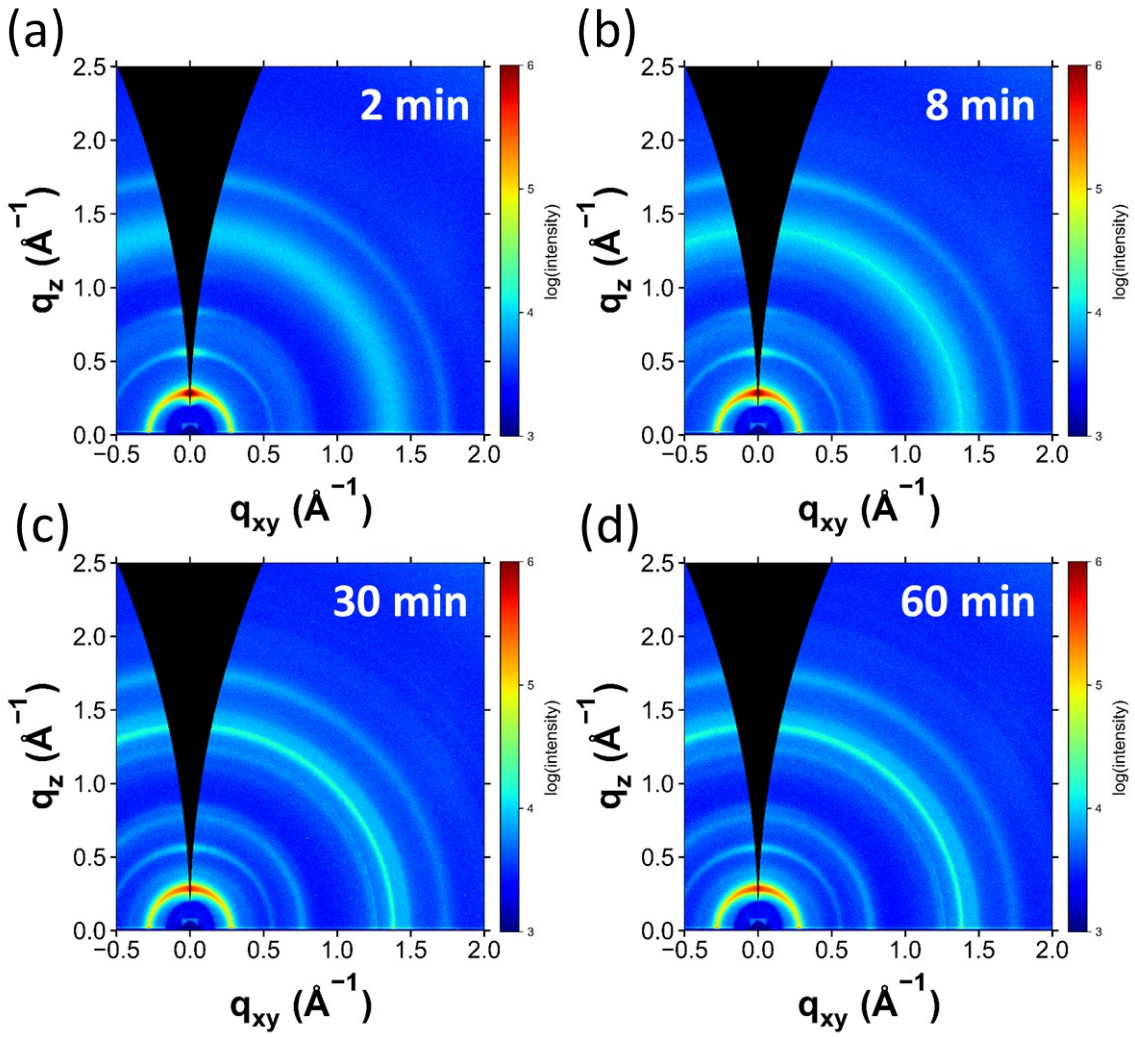

Fig. S8 Representative GIWAXS scattering patterns of spin-coated PCE11:PCBM 1:1.2 w:w 300 nm thick film thermally annealed at 130 °C for: (a) 2 min, (b) 8 min, (c) 30 min and (d) 60 min. PCBM crystallization starts between 2 and 8 minutes.

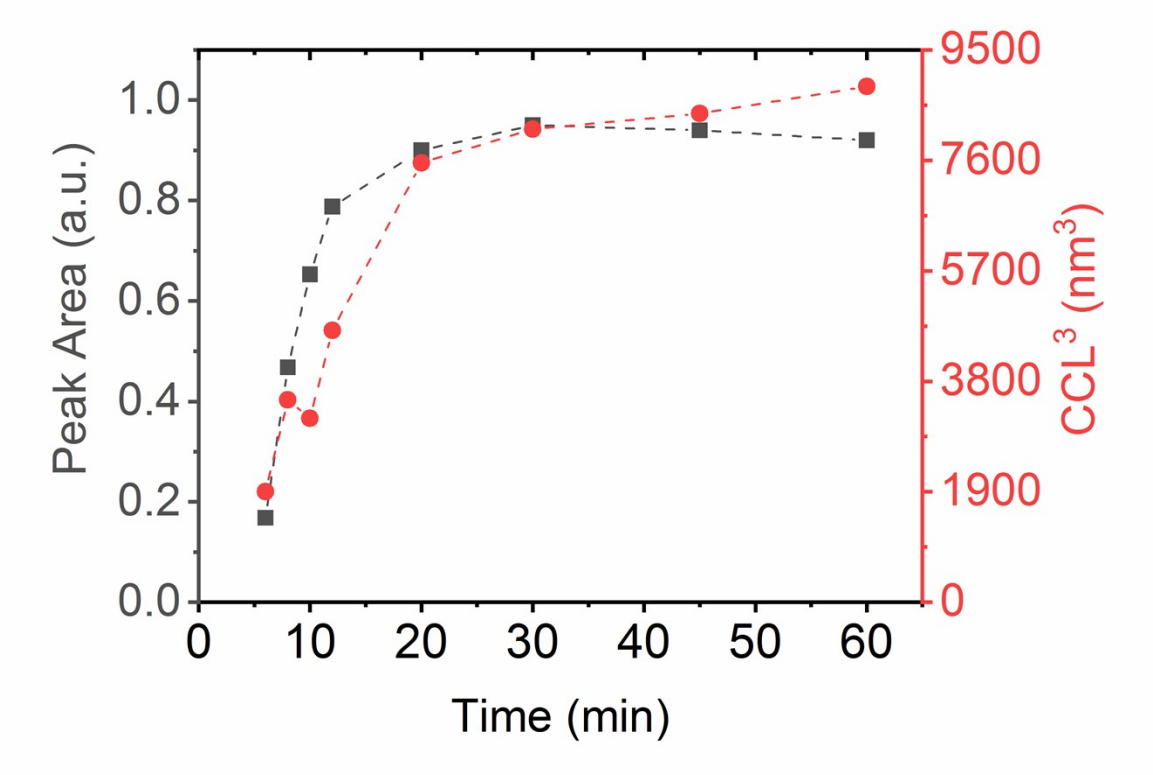

Fig. S9 The Peak area and the 3rd power of the crystal coherence length (CCL^3) of the PCBM q = 1.39 A^{-1} peak in the GIWAXS patterns of 300 nm thick spin-coated PCE11:PCBM 1:1.2 w:w films during thermal annealing at 130 °C. The peak area is proportional to the degree of PCBM crystallinity in the film.

The crystal coherence length (CCL) of PCBM was calculated from Scherrer's equation:[10]

$$CCL = \frac{2\pi}{FWHM}$$

Where FWHM is the full-width-at-half-maximum of the crystalline PCBM peak at q = 1.38 A^{-1}. The CCL is commonly used as a proxy for the size of the crystalline domains with all other morphological features being equal.[11]

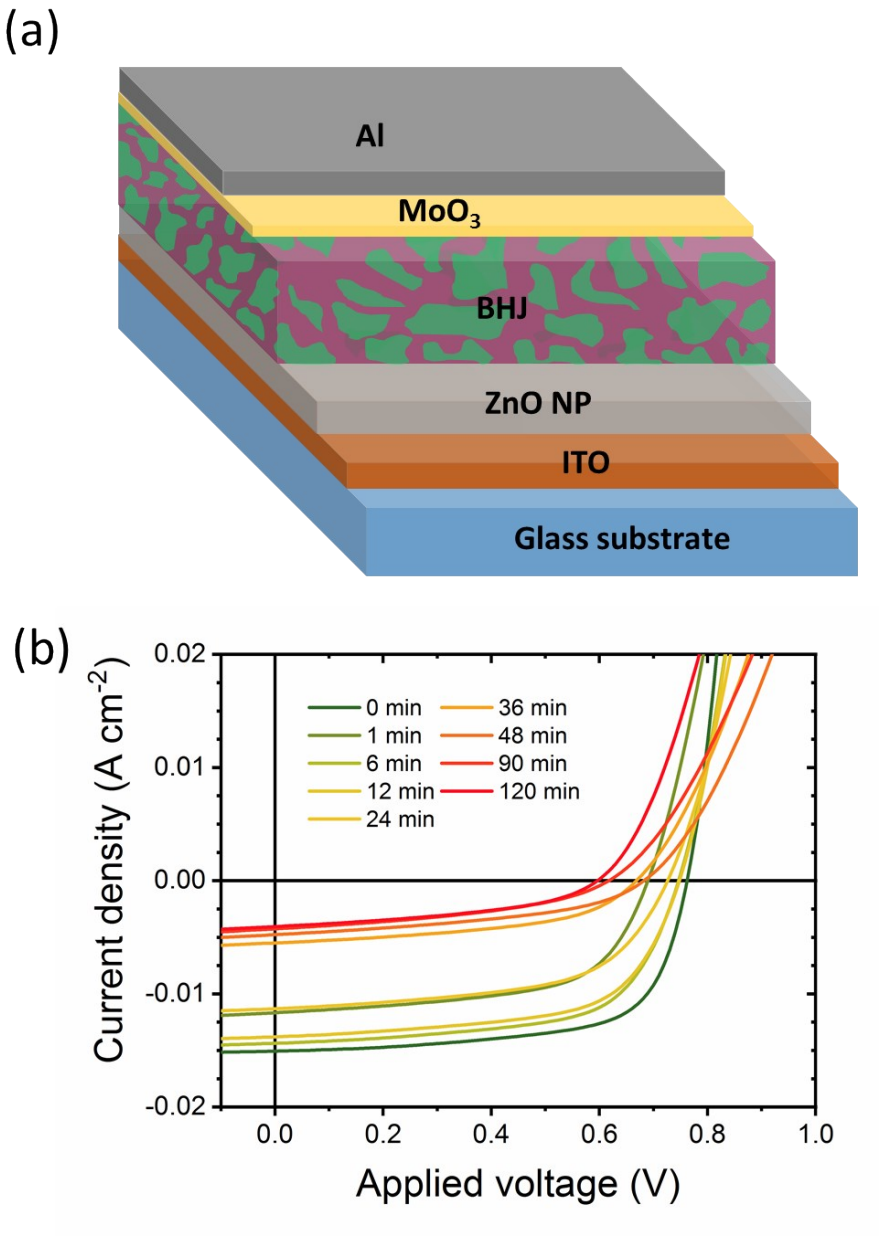

Fig. S10 Structure and performance of the PCE11:PCBM OSCs: (a) Schematic illustration of the device structure. (b) OSC J-V characteristics as a function of annealing time at 130 °C (1 – 120 min). The J-V measurements were acquired under 100 mW cm^{-2} AM1.5G irradiation.

Table S1 Average OSC photovoltaic parameters as a function of annealing time at 130 °C (1 – 120 min) extracted from the J-V curves in Fig. S11b. For each temperature at least 6 devices were measured and the error represent the standard deviation.

Time (min)	J_{sc} (mA cm^{-2})	FF	V_{oc} (V)	PCE (%)
0	15.07 ± 0.36	0.76 ± 0.00	0.67 ± 0.02	7.42 ± 0.09
1	11.67 ± 0.24	0.69 ± 0.03	0.60 ± 0.03	4.81 ± 0.42
6	14.37 ± 0.62	0.75 ± 0.01	0.63 ± 0.01	6.67 ± 0.39
12	13.80 ± 0.36	0.75 ± 0.00	0.62 ± 0.04	6.34 ± 0.57
24	11.32 ± 0.23	0.73 ± 0.01	0.58 ± 0.01	4.59 ± 0.10
36	5.50 ± 0.20	0.67 ± 0.01	0.49 ± 0.02	1.76 ± 0.13
48	4.77 ± 0.40	0.68 ± 0.02	0.44 ± 0.04	1.39 ± 0.17
90	4.26 ± 0.09	0.61 ± 0.02	0.41 ± 0.03	1.05 ± 0.11
120	4.05 ± 0.28	0.60 ± 0.01	0.43 ± 0.03	1.02 ± 0.15

References

1 C. Lindqvist, E. Wang, M. R. Andersson and C. Müller, *Macromol. Chem. Phys.*, 2014, **215**, 530–535.

2 Y. Zhang, A. J. Parnell, F. Pontecchiani, J. F. K. Cooper, R. L. Thompson, R. A. L. Jones, S. M. King, D. G. Lidzey and G. Bernardo, *Sci. Rep.*, 2017, **7**, 44269.

3 C. Müller, *Chem. Mater.*, 2015, **27**, 2740–2754.

4 C. Lindqvist, A. Sanz-Velasco, E. Wang, O. Bäcke, S. Gustafsson, E. Olsson, M. R. Andersson and C. Müller, *J. Mater. Chem. A*, 2013, **1**, 7174–7180.

5 H. W. Ro, J. M. Downing, S. Engmann, A. A. Herzing, D. M. DeLongchamp, L. J. Richter, S. Mukherjee, H. Ade, M. Abdelsamie, L. K. Jagadamma, A. Amassian, Y. Liu and H. Yan, *Energy Environ. Sci.*, 2016, **9**, 2835–2846.

6 M. Fox, *Optical properties of solids*, Oxford University Press, Oxford, England, 2nd ed., 2010.

7 W. R. Wu, U. S. Jeng, C. J. Su, K. H. Wei, M. S. Su, M. Y. Chiu, C. Y. Chen, W. Bin Su, C. H. Su and A. C. Su, *ACS Nano*, 2011, **5**, 6233–6243.

8 J. L. Allen, T. R. Jow and J. Wolfenstine, *Chem. Mater.*, 2007, **19**, 2108–2111.

9 J. W. Christian, *The theory of transformations in metals and alloys*, Pergamon, Amsterdam, 3rd ed., 2002.

10 R. J. Roe, *Methods of X-ray and neutron scattering in polymer science* , Oxford University Press, New York, 2000.

11 J. Rivnay, S. C. B. Mannsfeld, C. E. Miller, A. Salleo and M. F. Toney, *Chem. Rev.*, 2012, 112, 5488–5519.